Micromechanical Model for the Orthotropic Elastic Constants of Polyetheretherketone Composites Considering the Orientation Distribution of the Hydroxyapatite Whisker Reinforcements

Justin M. Deuerling[1]
J. Scott Vitter[2]
Gabriel L. Converse[3]
Ryan K. Roeder[4]
e-mail: rroeder@nd.edu

Department of Aerospace and Mechanical Engineering,
Bioengineering Graduate Program,
148 Multidisciplinary Research Building,
University of Notre Dame,
Notre Dame, IN 46556

Hydroxyapatite (HA) whisker reinforced polyetheretherketone (PEEK) composites have been investigated as bioactive materials for load-bearing orthopedic implants with tailored mechanical properties governed by the volume fraction, morphology, and preferred orientation of the HA whisker reinforcements. Therefore, the objective of this study was to establish key structure-property relationships and predictive capabilities for the design of HA whisker reinforced PEEK composites and, more generally, discontinuous short fiber-reinforced composite materials. HA whisker reinforced PEEK composites exhibited anisotropic elastic constants due to a preferred orientation of the HA whiskers induced during compression molding. Experimental measurements for both the preferred orientation of HA whiskers and composite elastic constants were greatest in the flow direction during molding (3-axis, C_{33}), followed by the transverse (2-axis, C_{22}) and pressing (1-axis, C_{11}) directions. Moreover, experimental measurements for the elastic anisotropy and degree of preferred orientation in the same specimen plane were correlated. A micromechanical model accounted for the preferred orientation of HA whiskers using two-dimensional implementations of the measured orientation distribution function (ODF) and was able to more accurately predict the orthotropic elastic constants compared to common, idealized assumptions of randomly oriented or perfectly aligned reinforcements. Model predictions using the 3-2 plane ODF, and the average of the 3-1 and 3-2 plane ODFs, were in close agreement with the corresponding measured elastic constants, exhibiting less than 5% average absolute error. Model predictions for C_{11} using the 3-1 plane ODF were less accurate, with greater than 10% error. This study demonstrated the ability to accurately predict differences in orthotropic elastic constants due to changes in the reinforcement orientation distribution, which will aid in the design of HA whisker reinforced PEEK composites and, more generally, discontinuous short fiber-reinforced composites. [DOI: 10.1115/1.4005421]

Keywords: anisotropy, discontinuous fiber-reinforced composites, elastic constants, hydroxyapatite, micromechanical model, orientation distribution function, polyetheretherketone, texture

1 Introduction

The mechanical properties of discontinuous, short fiber-reinforced composite materials are governed by the volume fraction, morphology, and arrangement of the reinforcement phase. The ability to predict and tailor the elastic properties of composite biomaterials is important for implant design. For example, an implant of greater stiffness relative to the peri-implant tissue can lead to stress shielding, osteolysis, and failure due to loosening [1–4]. On the other hand, an overly compliant implant may fail due to an inability to bear the required levels of load [4,5]. The implant stiffness may be designed considering both the implant geometry and material properties. Due to dimensional constraints imposed by human anatomy, material properties may be desired to match or slightly exceed those of the host tissue.

Hydroxyapatite (HA) reinforced polyetheretherketone (PEEK) composites have been investigated for use in load-bearing orthopedic applications [6–8]. PEEK is biocompatible, bioinert, radiolucent, and exhibits high strength and similar compliance to bone. These favorable properties have contributed to clinical use in interbody cages and posterior pedicle fixation rods for spinal fusion, as well as femoral stems in total hip arthroplasty [8–11]. However, PEEK alone is not bioactive but encapsulated by fibrous tissue rather than direct bone apposition [7,12]. Therefore, in

[1]Engineer II, Sports Medicine, R&D, RTI Biologics, 11621 Research Circle, Alachua, FL 32615.
[2]Engineer Platoon Leader, United States Army, 2003 Palmer Court, Lawrence, KS 66047.
[3]Director of Bioengineering, Cardiac Surgical Research Laboratories, Children's Mercy Hospital, Kansas City, MO 64108.
[4]Corresponding author.
Contributed by the Materials Division of ASME for publication in the JOURNAL OF ENGINEERING MATERIALS AND TECHNOLOGY. Manuscript received August 11, 2011; final manuscript received October 10, 2011; published online December 12, 2011. Assoc. Editor: Dongsheng Li.

spinal fusion, for example, autograft or recombinant human bone morphogenetic protein (e.g., rhBMP-2) is required for osteointegration [9]. There is also limited ability to tailor the mechanical properties of PEEK for a particular implant design or to match the peri-implant tissue. HA reinforcements provide bioactivity and the ability to tailor the mechanical properties of PEEK through control of the reinforcement volume fraction, morphology, and preferred orientation [7].

Dense and porous PEEK composites reinforced with HA whiskers have achieved mechanical properties similar to those of cortical and trabecular bone, respectively [13–15]. Dense HA whisker reinforced PEEK composites exhibited a preferred orientation of the HA whiskers with respect to the flow direction during compression molding and anisotropic elastic constants [13]. A micromechanical model that accounted for the orientation distribution of HA whiskers in similar high density polyethylene (HDPE) composites was shown to more accurately predict the magnitude and anisotropy of elastic constants compared to common assumptions of randomly oriented or perfectly aligned reinforcements [16]. The orientation distribution of the single crystal HA whiskers was measured using quantitative X-ray texture analysis [13,16], which is the most common and accurate method to measure the preferred orientation of grains in polycrystalline materials and single crystal reinforcements in composite materials [17]. The degree of preferred orientation is measured by differences in the relative integrated intensity of crystallographic reflections in X-ray diffraction (XRD) spectra for textured versus randomly oriented specimens. Measurements taken over the entire orientation space are interpolated to calculate an orientation distribution function (ODF), which is a statistical function describing the relative probability for a volume of crystals having a given angle of misorientation [17]. Synthetic and biological HA has a hexagonal crystal structure and the 001 crystallographic direction, or *c*-axis, is coincident with the long axis of HA whiskers [18–20]. Therefore, quantitative measurement of a 001 crystallographic texture for HA is equivalent to the morphological texture, that is, the alignment of HA whisker long axes, and the ODF can be used as a weight function to average the contribution of misoriented representative volume elements (RVEs) when calculating effective elastic constants [16,21].

The aims of this study were to (1) characterize the preferred orientation of HA whiskers within the PEEK matrix of bone-mimetic composites using quantitative X-ray texture analysis, (2) correlate measurements of the preferred orientation of HA whiskers with the elastic anisotropy of the composites, and (3) predict the anisotropic elastic constants using a micromechanical model accounting for the volume fraction, morphology, and preferred orientation of HA whiskers in the PEEK matrix. These aims contributed to a broader objective to establish key structure-property relationships and predictive capabilities for the design of HA whisker reinforced PEEK composites and, more generally, discontinuous short fiber-reinforced composite materials.

2 Materials and Methods

2.1 Composite Processing. A total of fifteen, $2.6 \times 5 \times 5$ mm specimens were machined from HA reinforced PEEK composite bars containing 10, 20, 30, 40, or 50 vol. % HA whiskers (Fig. 1(*a*)). Composites were manufactured using methods described in detail elsewhere [13]. Briefly, HA whiskers were synthesized using the chelate decomposition method [22,23] and exhibited a length of 21.6 (+16.9/−9.5) μm, a width of 2.8 (+0.8/−0.6) μm, and an aspect ratio of 7.6 (+5.7/−3.2), where the reported values correspond to the mean (± standard deviation) of a log-normal distribution [13]. As-synthesized HA whiskers and a commercially available PEEK powder (150XF, Victrex USA Inc., Greenville, SC) were codispersed in ethanol, dried, cold-pressed into a powder compact, and then compression molded into $2.6 \times 10 \times 125$ mm composite bars in an open channel die at 345–350 °C. A Cartesian coordinate system was employed with the 1, 2, and 3 specimen axes coincident with the press, transverse, and flow directions during molding, respectively (Fig. 1(*a*)).

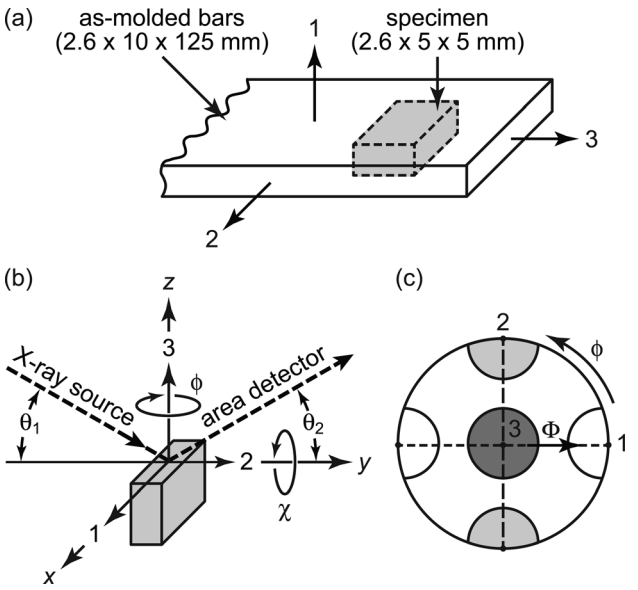

Fig. 1 (*a*) HA whisker reinforced PEEK specimens were sectioned from the center of compression molded composite bars with the 1, 2, and 3 specimen axes coincident with the press, transverse, and flow directions, respectively, during compression molding. (*b*) For pole figure measurements using XRD, the specimen was positioned using a 1/4-circle Eulerian cradle goniometer with the 1, 2, and 3 specimen axes initially aligned with the *x*-, *y*-, and *z*-axes of the goniometer, respectively. The Bragg angles, 2θ ($2\theta = \theta_1 + \theta_2$), tilt angle, χ, and rotation angle, ϕ, correspond to rotations about the goniometer axes. (*c*) Stereographic projection showing the showing specimen axes and Euler angles. Dashed lines show 2D implementations of the ODF in the 3-1 and 3-2 specimen planes for use in the micromechanical model. The 3-T ODF was averaged about ϕ. A scalar measure of the degree of preferred orientation was taken as the volume fraction of HA whiskers with *c*-axes oriented within 30 deg of the 1, 2, and 3 specimen axes, as shown.

2.2 Composite Elastic Constants. Elastic constants were measured in each of the three orthogonal specimen axes using the pulse-transmission method for ultrasonic wave propagation, as described in detail elsewhere [13]. The first three elastic constants (C_{11}, C_{22}, and C_{33}) from the main diagonal of the reduced fourth-order stiffness tensor were measured as

$$C_{ii} = \rho \cdot v_{ii}^2 (i = 1, 2, 3) \tag{1}$$

where ρ is the apparent density of the specimen and v_{ii} is the wave velocity in the ith specimen direction. The apparent density of each specimen was measured by Archimedes principle as

$$\rho_{app} = \frac{M}{M - s} \cdot \rho_w \tag{2}$$

where M is the mass of the specimen when saturated with deionized water, S is the apparent mass when suspended in deionized water, and ρ_w is the density of deionized water [24]. The ultrasonic wave velocity was measured using a pulse generator and 2.25 MHz transducers (Models 5800 and V106RM, Panametrics, Inc., Waltham, MA) as $v_{ii} = d_i/\Delta t$, where d_i is the specimen dimension measured using digital calipers (± 0.01 mm accuracy) and Δt is the time delay for wave transmission measured using an oscilloscope (± 10 ns accuracy). Deionized water was used as a couplant.

Elastic anisotropy ratios were defined as the ratio of elastic constants in the 3-1 and the 3-2 specimen planes. The elastic anisotropy ratio in the 1-2 plane was not independent of the other two ratios and was therefore omitted from analyses. A 3-T elastic anisotropy ratio was calculated as the mean of the 3-1 plane and 3-2 plane anisotropy ratios to account for an assumption of transverse isotropy in which the transverse elastic constants (1-2 plane) were constrained to be equal.

2.3 HA Whisker Aspect Ratio. The aspect ratio of HA whiskers in a thermoplastic matrix was previously shown to be degraded during compression molding [16]. Therefore, the aspect ratio of HA whiskers after compression molding was measured by ashing specimens at 600 °C to pyrolize the PEEK matrix without altering the HA whisker morphology. Microscopy slides were prepared by ultrasonically dispersing a 30 mg sample of the residual HA whiskers in 10 mL of ethanol and pipetting drops of the dispersion onto a microscope slide placed in an oven at 90 °C to quickly evaporate the ethanol. The length and width of HA whiskers were measured using standard stereological methods on digitized images (ImageJ, National Institutes of Health) taken at 400 × magnification with a transmitted light microscope (Eclipse ME600, Nikon Instruments, Inc., Melville, NJ). A 9 × 12 square grid was digitally overlaid using the image analysis software to facilitate random selection of HA whiskers located at grid nodes. The aspect ratio was calculated by dividing the whisker length by the width for a total of 500 whiskers per sample for composites reinforced with 10–50 vol. % HA whiskers.

2.4 HA Whisker Orientation Distribution. The orientation distribution of single crystal HA whiskers was measured for each specimen by quantitative texture analysis using an X-ray diffractometer equipped with an area detector (D8 Discover with general area detector diffraction system (GADDS), HI-STAR, Bruker AXS, Inc., Madison, WI). The specimen face normal to the 3-axis was polished to a 3 μm finish using a series of diamond compounds. Specimens were mounted on a $^1/_4$-circle Eulerian cradle goniometer that allowed accurate 6-axis positioning of the polished specimen face normal to the 3-axis (Fig. 1(*b*)). Monochromatic Cu Kα radiation was generated at 40 kV and 40 mA, and focused on the specimen face by a 0.5 mm diameter pinhole collimator with the assistance of a laser-video microscope. The sample to detector distance was set at 15 cm.

Pole figures were measured for specimens by XRD using the scheme summarized in Table 1. The θ_1 and θ_2 goniometer angles were each set to 27.5 deg such that the center of the detector was at $2\theta = 55$ deg. This allowed for simultaneous measurement of pole figures for the 222 ($2\theta = 46.711$ deg), 213 ($2\theta = 49.468$ deg), and 004 ($2\theta = 53.143$ deg) crystallographic reflections. These crystallographic reflections were selected for their relative intensity, separation from neighboring peaks, and location in the orientation space. Two-dimensional (2D) X-ray spectra were measured in scanning mode for 12 deg increments in ϕ at $\chi = 73$ deg for 3 min/frame and for 9 deg increments in ϕ at $\chi = 40$ deg for 6 min/frame (Table 1). The specimens were oscillated in the 1-2 plane during scans to maximize the sampled specimen volume while maintaining a constant diffraction plane. Pilot studies verified that this data collection scheme provided adequate resolution and pole sphere coverage for accurate and precise construction of pole figures.

Table 1 XRD data collection scheme for pole figures measuring the preferred orientation of single crystal HA whiskers in the PEEK matrix. The Bragg angles, 2θ ($2\theta = \theta_1 + \theta_2$), tilt angle, χ, and rotation angle, ϕ, are shown schematically in Fig. 1(*b*)

θ_1 (deg)	θ_2 (deg)	(χ deg)	$\Delta\phi$ (deg)	Frames	Time/frame (min)	Reflection	2θ (deg)
27.5	27.5	73	12	30	3	222	46.711
						213	49.468
						004	53.143
27.5	27.5	40	9	40	6	222	46.711
						213	49.468
						004	53.143

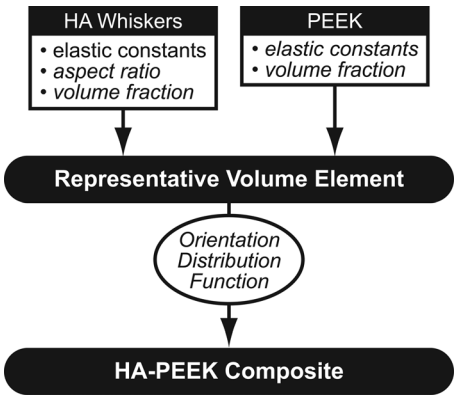

Fig. 2 Schematic diagram of the micromechanical model used to predict the anisotropic elastic constants of HA whisker reinforced PEEK composites. Structural parameters in *italics* were experimentally measured

Experimental pole figures were constructed from the X-ray spectra by integrating the 2D frames in 2θ over each peak of interest after subtracting the background intensity (GADDS v4.1). Pole figures were interpolated and subsequently normalized by pole figures measured for composite specimens reinforced with randomly oriented, equiaxed HA powder reinforcements. ODFs were calculated from the normalized pole figures by the arbitrarily defined cells (ADC) method (LaboTex, v2.1, LaboSoft s.c., Poland). Finally, pole figures and inverse pole figures were recalculated from ODFs and plotted to show the orientation distribution. A scalar measure of the degree of preferred orientation was taken as the volume fraction of HA whiskers with *c*-axes oriented within 30 deg of the 1, 2, and 3 specimen axes and termed the oriented crystal fraction (Fig. 1(*c*)). For correlation with the elastic anisotropy ratios, oriented crystal ratios were defined as the ratio of the oriented crystal fractions in the 3-1 and 3-2 planes.

2.5 Micromechanical Model. A micromechanical model (Fig. 2) was adapted from previous studies [16,21]. Briefly, elastic constants for a RVE comprising discontinuous, aligned square fiber reinforcements (HA whiskers) within a continuous PEEK matrix were modeled using Halpin-Tsai equations [25]. Halpin-Tsai equations accounted for the elastic constants and known volume fractions of the constituent phases, as well as the measured aspect ratio of HA whiskers at each reinforcement level. Isotropic elastic constants for the PEEK matrix were measured using ultrasonic wave propagation on unreinforced PEEK specimens, and elastic constants for HA single crystals were taken from data in the literature [26]. Effective elastic constants for HA whisker reinforced PEEK composites were then calculated by averaging the weighted contribution of all misoriented RVEs by the experimentally measured ODF as

$$\bar{C} = \frac{\int C_{RVE}(R,\theta) \cdot f(R) \cdot g(\theta) \cdot dR \cdot d\theta}{\int f(R) \cdot g(\theta) \cdot dR \cdot d\theta} \tag{3}$$

where R is the HA whisker aspect ratio, θ is the angle of misorientation between the specimen 3-axis and HA whisker *c*-axes, $f(R)$ is the aspect ratio distribution, $g(\theta)$ is the ODF, and $C_{\mathrm{RVE}}(R,\theta)$ is the stiffness tensor computed for the misoriented RVE in the sample coordinate system after tensor transformation through θ. The prediction of orthotropic and transversely isotropic elastic

constants was facilitated by computing 2D ODFs for the 3-1, 3-2, and 3-T specimen planes from the measured three-dimensional (3D) ODF (Fig. 1(*c*)). Model predictions for elastic constants in the transverse plane using ODFs for the 3-1, 3-2, and 3-T specimen planes were compared to experimental measurements for C_{11}, C_{22}, and their average, C_T, respectively.

2.6 Statistical Methods. Two-way analysis of variance (ANOVA, STATVIEW 5.0.1, SAS Institute, Inc., Cary, NC) was used to examine the effects of the reinforcement volume fraction and specimen axis on the measured elastic constants and oriented crystal volume fractions. *Post hoc* comparisons were performed using a Tukey–Kramer test. One-way ANOVA with a Tukey–Kramer *post hoc* test was used to examine the effect of the reinforcement volume fraction on the HA whisker aspect ratio measured after compression molding. Linear least squares regression was used to correlate elastic anisotropy ratios with the oriented crystal ratios and elastic constant magnitudes with the corresponding micromechanical model predictions. Paired and unpaired Student's *t*-tests were used to compare experimental data to model predictions. The level of significance for all tests was set at $p < 0.05$.

3. Results

3.1 Experimental Results. Elastic constants in all three specimen axes increased significantly with increased HA volume fraction ($p < 0.0001$, ANOVA), as expected (Fig. 3, Table 2). Elastic constants also exhibited orthotropy at reinforcement levels greater than 20 vol. % with $C_{33} > C_{22} > C_{11}$ ($p < 0.05$, Tukey–Kramer) (Fig. 3). The C_{33}/C_{11} elastic anisotropy ratio was significantly greater than C_{33}/C_{22} ($p < 0.0001$, ANOVA), and both were not dependent on the HA volume fraction ($p = 0.37$, ANOVA) (Table 2).

The HA whisker aspect ratio distribution in compression molded composites was log-normal ranging from 1 to 8. The mean (± standard deviation) aspect ratio was degraded from 7.6 (+5.7/−3.2) as-synthesized to 2.5 (+1.2/−0.8) in compression molded PEEK composites pooled across all HA volume fractions. The mean aspect ratio of compression molded composites with 20 vol. % HA whiskers was statistically different ($p < 0.05$, Tukey–Kramer) from other reinforcement levels, but the magnitude of all differences was less than 0.2.

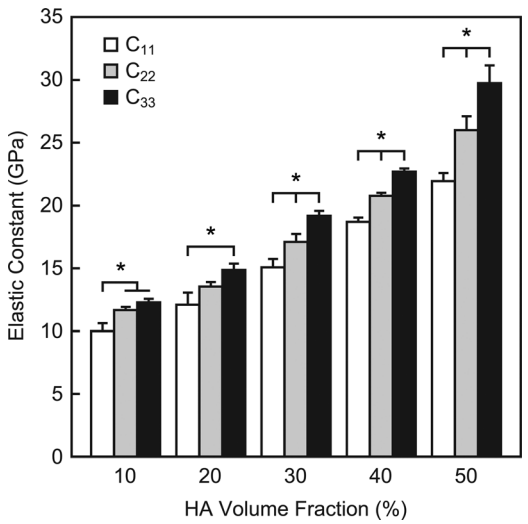

Fig. 3 Elastic constants measured in each of the three principal specimen axes (C_{11}, C_{22}, and C_{33}) of PEEK composites increased with increased HA whisker volume fraction ($p < 0.0001$, ANOVA) and exhibited orthotropic symmetry at reinforcement levels greater than 20 vol. %, with $C_{33} > C_{22} > C_{11}$ (*$p < 0.05$, Tukey–Kramer). Error bars show one standard deviation. Experimental data are given in Table 2.

Table 2 Mean (± standard deviation) elastic constants (C_{11}, C_{22}, and C_{33}) and anisotropy ratios (C_{33}/C_{11} and C_{33}/C_{22}) measured for HA whisker reinforced PEEK composites

HA content (vol. %)	C_{11} (GPa)	C_{22} (GPa)	C_{33} (GPa)	C_{33}/C_{11}	C_{33}/C_{22}
10	10.0 (0.6)	11.7 (0.3)	12.3 (0.3)	1.23 (0.05)	1.05 (0.01)
20	12.1 (1.0)	13.5 (0.4)	14.9 (0.5)	1.23 (0.06)	1.10 (0.07)
30	15.1 (0.7)	17.1 (0.6)	19.2 (0.4)	1.27 (0.04)	1.12 (0.05)
40	18.7 (0.3)	20.8 (0.2)	22.7 (0.3)	1.21 (0.03)	1.09 (0.02)
50	21.9 (0.7)	26.0 (1.1)	29.8 (1.4)	1.36 (0.06)	1.14 (0.02)

Pole figures for the 001, 010, and 100 crystallographic directions revealed that HA whiskers in the PEEK matrix exhibited a *c*-axis (001) preferred orientation in the specimen 3-axis as a result of the composite processing (Fig. 4). Therefore, the overall orientation distribution exhibited a 001 fiber texture, but a relatively weak 001 sheet texture was also evident in the 3-2 plane. The oriented crystal volume fraction was not correlated with the HA volume fraction ($p = 0.58$, ANOVA) and was therefore pooled across all reinforcement levels for each specimen axis. The oriented crystal fraction was greatest in the 3-axis, followed by the 2-axis and 1-axis ($p < 0.0001$, ANOVA) (Fig. 5).

Elastic anisotropy ratios were strongly correlated with oriented crystal ratios when data for the 3-1 and 3-2 planes were pooled ($p < 0.0001$, $R^2 = 0.60$) (Fig. 6). Considered separately, elastic anisotropy in the 3-1 plane exhibited a relatively strong correlation ($p < 0.05$, $R^2 = 0.33$) with the corresponding oriented crystal ratio, and the 3-2 plane exhibited a relatively weak correlation ($p = 0.08$, $R^2 = 0.22$).

3.2 Micromechanical Model Predictions. Micromechanical model predictions using the aspect ratio distribution were not significantly different compared to predictions using the mean aspect ratio; therefore, all results and predictions below utilized the mean aspect ratio. Micromechanical model predictions for the longitudinal (C_{33}) and transverse (C_{11}, C_{22}, or the average, C_T) elastic constants were generated based upon each 2D implementation of the ODF (3-1 plane, 3-2 plane, and average 3-T), as well as idealized assumptions of randomly oriented or perfectly aligned HA whiskers. Model predictions using the measured ODFs more accurately predicted the experimental data compared to either of the common idealized assumptions, based upon the average absolute error (Table 3). Moreover, C_{33} was accurately predicted using any of the 2D implementations of the ODF. Model predictions for C_{22} using the 3-2 plane ODF were also accurate, but model predictions for C_{11} using the 3-1 plane ODF were less accurate, with greater than 10% error.

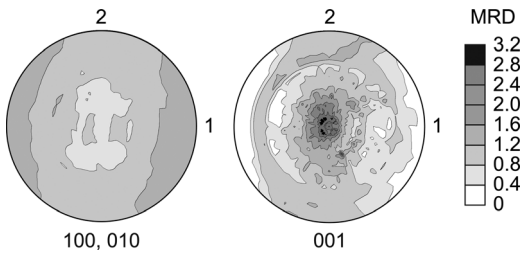

Fig. 4 Representative recalculated pole figures for a PEEK composite reinforced with 50 vol. % HA whiskers showing a *c*-axis (001) preferred orientation in the specimen 3-axis. There was also a weaker *c*-axis (001) preferred orientation in the specimen 2-axis relative to the 1-axis. The orientation distribution is shown in units of multiples of a random distribution (MRD), where MRD = 1 corresponds to a random distribution

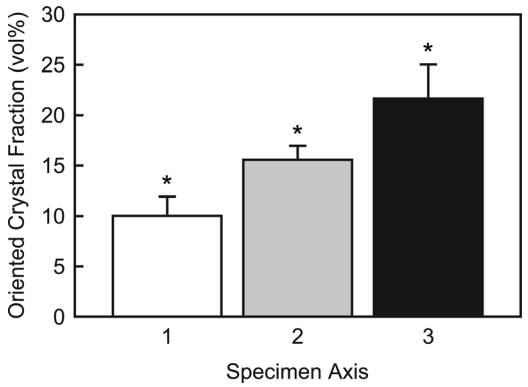

Fig. 5 The volume fraction of HA whisker crystals in the PEEK matrix oriented within 30 deg of each specimen axis was greatest in the 3-axis, followed by the 2-axis and 1-axis. Data was pooled across all reinforcement levels. Error bars show one standard deviation. Asterisks indicate a statistically significant difference from all other axes ($p < 0.05$, Tukey–Kramer)

Linear least squares regression showed strong correlations between model predictions which employed measured ODFs and corresponding experimental data (Fig. 7). The slope and intercept of regression lines were not statistically different from unity and zero, respectively, for predictions of the longitudinal elastic constant using any ODF and predictions of the transverse elastic constant using the 3-2 plane ODF (slope: $p > 0.20$, intercept: $p > 0.17$) (Fig. 7). A slope of unity and intercept of zero indicates an exact prediction of the experimental data. Model predictions of C_{33} using the 3-1 plane ODF ($p = 0.09$, paired t-test) and C_{22} using the 3-2 plane ODF ($p = 0.79$, paired t-test) were not statistically different from experimental data. All other predictions exhibited statistically significant differences from experimental data ($p < 0.05$, paired t-test) though the average error may have been less than 5% (Fig. 7).

Micromechanical model predictions were also compared to experimental data at each reinforcement level (Fig. 8). Experimental data and model predictions using measured ODFs were located at or between the upper and lower bounds represented by model predictions assuming perfectly aligned and randomly oriented HA whiskers. Interestingly, model predictions for C_{33} using each 2D implementation of the ODF were not significantly different from

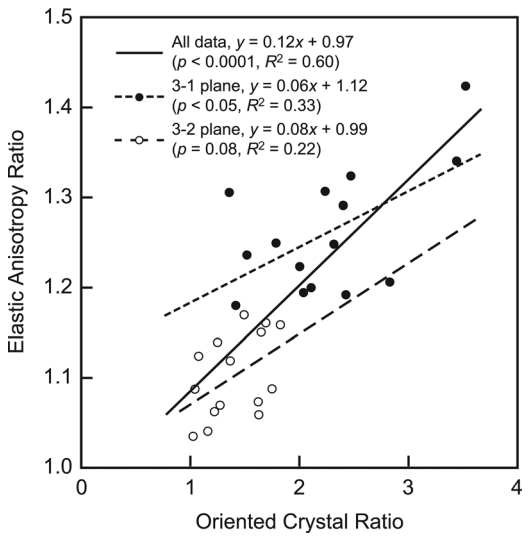

Fig. 6 The measured elastic anisotropy ratio of PEEK composites increased with an increased preferred orientation of HA whiskers, as measured by the oriented crystal ratio

Table 3 Average absolute error between micromechanical model predictions and experimental measurements of elastic constants and anisotropy ratios using various implementations of 2D ODFs or idealized assumptions. Note that model predictions for elastic constants in the transverse plane using ODFs for the 3-1, 3-2, and 3-T specimen planes were compared to experimental measurements for C_{11}, C_{22}, and their average, C_T, respectively

		Average absolute error (%)		
ODF used in model		C_{33}	C_T	C_{33}/C_T
Measured	3-1 Plane	3.6	11.5	12.4
	3-2 Plane	4.7	2.9	4.1
	Average 3-T	4.0	4.8	7.5
Idealized	Randomly oriented	7.5	8.8	14.8
	Perfectly aligned	13.7	5.7	20.4

experimental data at 20, 40, and 50 vol. % HA reinforcement, but were significantly different from the experimental data at 10 and 30 vol. % HA reinforcement (Fig. 8). At all reinforcement levels, experimental data for C_{11} and C_{22} were not statistically significantly different from model predictions assuming perfectly aligned HA or randomly oriented HA whiskers, respectively.

4 Discussion

This study demonstrated predictive capability for processing structure-property relationships in the design of HA whisker reinforced PEEK composites and, more generally, discontinuous short fiber-reinforced composites. Compression molding resulted in a preferred orientation of single crystal HA whiskers within the PEEK matrix. The preferred orientation was quantitatively characterized by an ODF (Fig. 4). The ODF was used in a micromechanical model to calculate the weighted average of misoriented RVEs (Eq. 3), which enabled significantly improved predictive capability over common idealized assumptions for reinforcement orientation within an RVE (Table 3).

HA whiskers were aligned by shear forces acting in directions of flow during compression molding of the viscous PEEK melt. Therefore, the preferred orientation of HA whiskers was greatest in the flow direction (3-axis), followed by the transverse (2-axis) and pressing (1-axis) directions (Figs. 1(*a*), 4, and 5). The predominance of the c-axis fiber texture in the specimen 3-axis was consistent with previous investigations of compression molded HA whisker reinforced PEEK [13] and HDPE [16] composites. Alignment of elongated reinforcements in directions of flow during injection and compression molding has also been characterized in short fiber-reinforced composites [27–30]. Through-thickness variation in the orientation distribution is common in short fiber-reinforced composites and was likely present in this study but was effectively averaged by the ODF measurement scheme. This simplification would be expected to have the greatest effect on predictions for C_{11} and may have been responsible for the greater inaccuracy of predictions for C_{11} in this study (Table 3, Figs. 7 and 8). Through-thickness variation in the preferred orientation could be modeled as a trilayer laminate with a more highly oriented skin and a less oriented core. Nonetheless, micromechanical model predictions for C_{11} were reasonably accurate despite assuming through-thickness homogeneity.

The measured orthotropic elastic constants were correlated to the HA whisker preferred orientation (Fig. 6). Elastic constants were greatest in the flow direction (3-axis), followed by the transverse (2-axis) and pressing (1-axis) directions (Figs. 1(*a*) and 3). PEEK composites reinforced with 30–50 vol. % HA whiskers exhibited similar elastic constant magnitudes but less anisotropy (Fig. 3, Table 2) compared to the range exhibited by human cortical bone tissue [31,32]. Therefore, the elastic anisotropy of HA

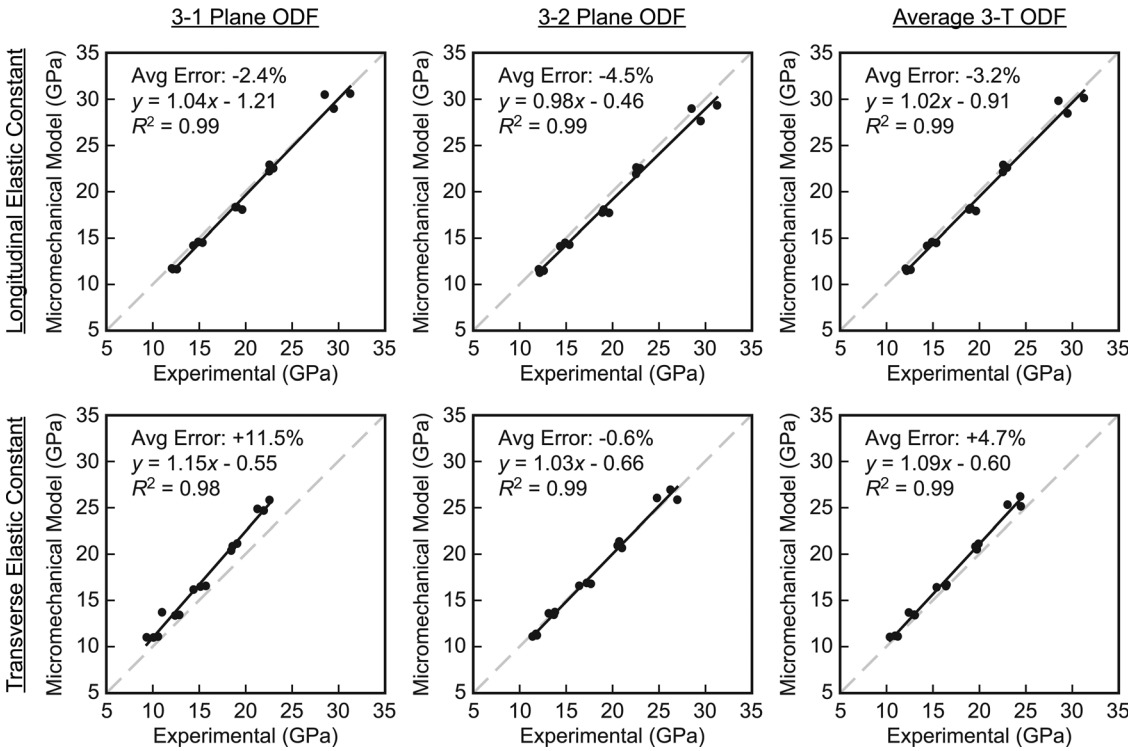

Fig. 7 Linear least squares regression revealed a strong correlation between micromechanical model predictions using 2D implementations of the measured ODF (3-1 plane, 3-2 plane, and average 3-T) and the corresponding experimental data ($p<0.0001$, $R^2>0.98$). Model predictions of C_{33} using the 3-1 plane ODF ($p=0.09$, paired *t*-test) and C_{22} using the 3-2 plane ODF ($p=0.79$, paired *t*-test) were not statistically different from experimental data. All other predictions exhibited statistically significant differences from experimental data ($p<0.05$, paired *t*-test) though the average error may have been less than 5%

whisker reinforced PEEK composites may be tailored by controlling the preferred orientation of HA whiskers. This could be achieved in practice by increasing the flow rate during compression molding to increase the shear forces acting to align the HA whiskers, or by changing the mold geometry to encourage or restrict flow.

Correlation of the oriented crystal ratio and elastic anisotropy ratio in the 3-1 plane alone and the pooled data was statistically significant with coefficient of determination (R^2) of 0.22 and 0.60, respectively, while in the 3-2 plane the relationship was not statistically significant ($p=0.08$, $R^2=0.22$) (Fig. 6). The strength of these correlations was limited by the number of specimens, as well as the small specimen volume sampled during X-ray diffraction compared to the total specimen volume. The entire polished specimen face was exposed to X-rays, but X-ray penetration depths are typically on the order of 100–500 μm [33]. Therefore, less than 10% of total specimen volume was sampled when measuring the ODF, whereas ultrasonic wave propagation sampled the entire specimen volume for elastic constants. The coefficient of variation for measurements of the oriented crystal ratio was 0.29 in the 3-1 plane and 0.20 in the 3-2 plane, which suggests that the structure-property correlation with anisotropy ratios could be improved if greater specimen volume were sampled. A larger specimen volume could be sampled by averaging texture measurements on serial sections. Neutron diffraction would also sample a greater volume due to an increased penetration depth compared to X-ray diffraction [17] but is limited in availability and requires long collection times.

The micromechanical model was able to predict orthotropic elastic constants using 2D implementations of the measured ODF in the 3-1 plane, 3-2 plane, and their average 3-T (Fig. 8). Model predictions using the 3-2 plane ODF and the average 3-T ODF were in close agreement with the corresponding experimentally measured elastic constants and more accurate compared to predictions using common idealized assumptions of randomly oriented or perfectly aligned reinforcements (Table 3, Fig. 8). However, model predictions for C_{11} using the 3-1 plane ODF were less accurate, often falling near the upper bound predicted using an assumption of randomly oriented HA whiskers (Table 3, Fig. 8). This error was not likely due to the 2D implementation of the ODF. As discussed above, through-thickness variation in the preferred orientation of HA whiskers likely resulted in a more highly oriented skin and a less oriented core that would be expected to most greatly influence C_{11}, but was not accounted for in this study. An assumption of perfect bonding between the matrix and reinforcements was implicit to the Halpin-Tsai equations and may have also contributed disproportionately to error in the prediction of C_{11} due to the narrow width of oriented HA whiskers. Another possible contribution to error in the prediction of C_{11} was that the PEEK matrix was assumed to be isotropic. The elastic constants for unreinforced PEEK, prepared and measured using the same methods as this study, were previously reported to be equivalent in the 3-2 plane, but C_{11} was slightly decreased [13]. Weak anisotropy in the PEEK matrix may have been due to alignment and/or crystallization of molecular chains during molding. This would also explain the proximity of measurements for C_{11} (3-1 plane) and C_{22} (3-2 plane) to model predictions assuming perfectly aligned and randomly oriented reinforcements, respectively.

The use of 2D implementations of the measured 3D ODF in the micromechanical model could be considered an advantage or a limitation. The 2D implementations simplified calculations by requiring only one misorientation angle and obviating the need to integrate over the entire Euler space. Considering a standard 5 deg discretization of the ODF, this amounts to a computational difference of averaging 19 points in orientation space versus 18,031

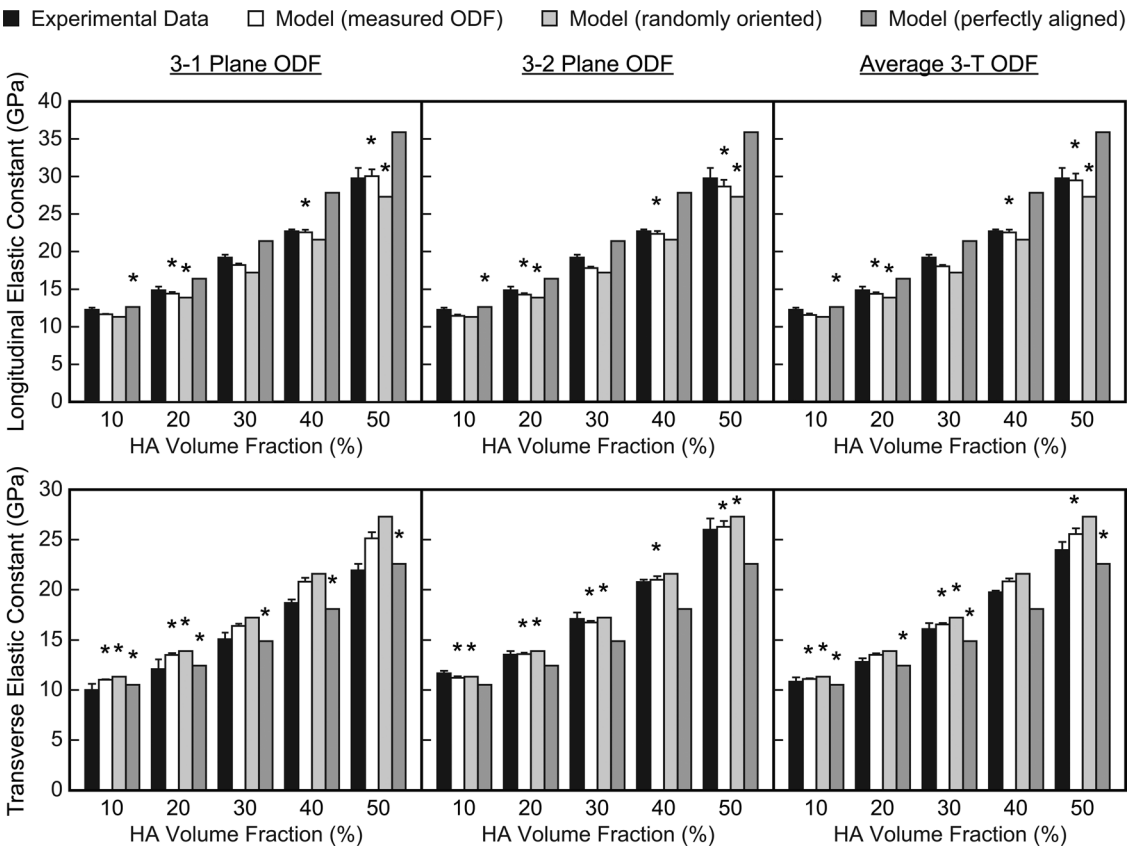

Fig. 8 Comparison of experimental data and micromechanical model predictions for the longitudinal and transverse elastic constants using 2D implementations of the measured ODF (3-1 plane, 3-2 plane, and average 3-T), as well as common idealized assumptions of randomly oriented or perfectly aligned whiskers. Error bars show one standard deviation. Asterisks indicate differences between model predictions and experimental data that are *not* statistically significant ($p > 0.05$, ANOVA). Model predictions using the 3-2 plane ODF and the average 3-T ODF were in close agreement with the corresponding measured elastic constants, exhibiting less than 5% average absolute error (Table 3). Model predictions for C_{11} using the 3-1 plane ODF were less accurate, with greater than 10% error (Table 3)

points. On the other hand, each 2D implementation was limited to making predictions in two directions, while the third was neglected. The micromechanical model can be readily extended in future work to integrate over the entire 3D ODF, enabling prediction of all three orthotropic elastic properties in a single model [34–36]. The accuracy of predictions using the full 3D ODF compared to those in this study would provide interesting insight into the importance and incorporation of orientation information in micromechanical models.

5 Conclusions

HA whisker reinforced PEEK composites exhibited anisotropic elastic constants due to the preferred orientation of the HA whiskers induced during compression molding. Experimental measurements for both the preferred orientation of HA whiskers and composite elastic constants were greatest in the flow direction during molding (3-axis), followed by the transverse (2-axis) and pressing (1-axis) directions. Moreover, experimental measurements for the elastic anisotropy and degree of preferred orientation in the same specimen plane were correlated. A micromechanical model accounted for the preferred orientation of HA whiskers using 2D implementations of the measured ODF and was able to more accurately predict the orthotropic elastic constants compared to common, idealized assumptions of randomly oriented or perfectly aligned reinforcements. Model predictions using the 3-2 plane ODF and the average 3-T ODF were in close agreement with the corresponding measured elastic constants, exhibiting less than 5% average absolute error. Model predictions for C_{11} using the 3-1 plane ODF were less accurate, with greater than 10% error. This study demonstrated the ability to accurately predict differences in orthotropic elastic constants due to changes in the reinforcement orientation distribution, which will aid in the design of HA whisker reinforced PEEK composites and, more generally, discontinuous short fiber-reinforced composites.

Acknowledgment

This research was partially supported by the U.S. Army Medical Research and Materiel Command (W81XWH-09-1-0741) and a Lilly Presidential Fellowship (JMD) from the University of Notre Dame.

References

[1] Bobyn, J. D., Mortimer, E. S., Glassman, A. H., Engh, C. A., Miller, J. E., and Brooks, C. E., 1992, "Producing and Avoiding Stress Shielding," Clin. Orthop. Relat. Res. **274**, pp. 79–96.
[2] Huiskes, R., Weinans, H., and van Rietbergen, B., 1992, "The Relationship Between Stress Shielding and Bone Resorption Around Total Hip Stems and the Effects of Flexible Materials," Clin. Orthop. Relat. Res. **274**, pp. 124–134.
[3] Vander Sloten, J., Labey, L., Van Audekercke, R., and Van der Perre, G., 1998, "Materials Selection and Design for Orthopaedic Implants with Improved Long-term Performance," Biomaterials, **19**, pp. 1455–1459.
[4] Latour, Jr., R. A., 1995, "Fiber-Reinforced Biomaterials for Orthopedic Implant Applications," *Encyclopedic Handbook of Biomaterials and Bioengineering, Part B: Applications*, D. L. Wise, D. J. Trantolo, D. E. Altobelli, M. J. Yaszemski, J. D. Gresser, E. R. Schwartz, eds., CRC Press, Boca Raton, Vol. 1, pp. 359–382.

[5] Rose, F. R. A. J., and Oreffo, R. O. C., 2002, "Bone Tissue Engineering: Hope vs. Hype," Biochem. Biophys. Res. Commun, **292**, pp. 1–7.
[6] Abu Bakar, M. S., Cheng, M. H. W., Tang, S. M., Yu, S. C., Liao, K., Tan, C. T., Khor, K. A., and Cheang, P., 2003, "Tensile Properties, Tension-tension Fatigue and Biological Response of Polyetheretherketone-hydroxyapatite Composites for Load-bearing Orthopedic Implants," Biomaterials, **24**, pp. 2245–2250.
[7] Roeder, R. K., and Conrad, T. L., 2011, "Bioactive Polyaryletherketone Composites," *PEEK Biomaterials Handbook*, S. M. Kurtz, ed., Elsevier, Inc., Amsterdam, pp. 163–179.
[8] Kurtz, S. M., and Devine, J. N., 2007, "PEEK Biomaterials in Trauma, Orthopedic, and Spinal Implants," Biomaterials, **28**, pp. 4845–4869.
[9] Toth, J. M., Wang, M., Estes, B. T., Scifert, J. L., Seim III, H. B., and Turner, A. S., 2006, "Polyetheretherketone as a Biomaterial for Spinal Applications," Biomaterials, **27**, pp. 324–334.
[10] Evans, S. L., and Gregson, P. J., 1998, "Composite Technology in Load-bearing Orthopaedic Implants," Biomaterials, **19**, pp. 1329–1342.
[11] Brantigan, J. W., McAfee, P. C., Cunningham, B. W., Wang, H., and Orbegoso, C. M., 1994, "Interbody Lumbar Fusion Using a Carbon Fiber Cage Implant Versus Allograft Bone," Spine, **19**, pp. 1436–1444.
[12] Von Wilmowsky, C., Lutz, R., Meisel, U., Srour, S., Rupprecht, S., Toyoshima, T., Nkenke, E., Shlegel, K. A., Pohle, D., Münstedt, H., Rechtenwald, T., and Schmidt, M., 2009, "*in vivo* Evaluation of β-TCP Containing 3D Laser Sintered Poly(ether ether ketone) Composites in Pigs," J. Bioact. Compat. Pol., **24**, pp. 169–184.
[13] Converse, G. L., Yue, W., and Roeder, R. K., 2007, "Processing and Tensile Properties of Hydroxyapatite-whisker-reinforced Polyetheretherketone," Biomaterials, **28**, pp. 927–935.
[14] Converse, G. L., Conrad, T. L., and Roeder, R. K., 2009, "Mechanical Properties of Hydroxyapatite Whisker Reinforced Polyetherketoneketone Composite Scaffolds," J. Mech. Behav. Biomed. Mater., **2**, pp. 627–635.
[15] Roeder, R. K., Smith, S. M., Conrad, T. L., Yanchak, N. J., Merrill, C. H., and Converse, G. L., 2009, "Porous and Bioactive PEEK Implants for Interbody Spinal Fusion," Adv. Mater. Process., **167**, pp. 46–48.
[16] Yue, W., and Roeder, R. K., 2006, "Micromechanical Model for Hydroxyapatite Whisker Reinforced Polymer Biocomposites," J. Mater. Res., **21**, pp. 2136–2145.
[17] Wenk, H.-R., and Houtte, P. V., 2004, "Texture and Anisotropy," Rep. Prog. Phys., **67**, pp. 1367–1428.
[18] Aizawa, M., Porter, A. E., Best, S. M., and Bonfield, W., 2005, "Ultrastructural Observation of Single-Crystal Apatite Fibers," Biomaterials, **26**, pp. 3427–3433.
[19] Yoshimura, M., Suda, H., Okamoto, K., and Ioku, K., 1994, "Hydrothermal Synthesis of Biocompatible Whiskers," J. Mater. Sci., **29**, pp. 3399–3402.
[20] Moradian-Oldak, J., Weiner, S., Addadi, L., Landis, W. J., and Traub, W., 1991, "Electron Imaging and Diffraction Study of Individual Crystals of Bone, Mineralized Tendon and Synthetic Carbonated Apatite," Connect. Tissue Res., **25**, pp. 219–228.
[21] Deuerling, J. M., Yue, W., Espinoza Orías, A. A., and Roeder, R. K., 2009, "Specimen-specific Multiscale Model for the Anisotropic Elastic Constants of Human Cortical Bone," J. Biomechanics, **42**, pp. 2061–2067.
[22] Roeder, R. K., Converse, G. L., Leng, H., and Yue, W., 2006, "Kinetic Effects on Hydroxyapatite Whiskers Synthesized by the Chelate Decomposition Method," J. Am. Ceram. Soc., **89**, pp. 2096–2104.
[23] Roeder, R. K., Sproul, M. S., and Turner, C. H., 2003, "Hydroxyapatite Whiskers Provide Improved Mechanical Properties in Reinforced Polymer Composites," J. Biomed. Mater. Res., **67A**, pp. 801–812.
[24] ASTM Standard C373-88, 1999, "Standard Test Method for Water Absorption, Bulk Density, Apparent Density and the Apparent Specific Gravity of Fired Whiteware Products," American Society for Testing Materials, West Conshohocken, PA.
[25] Halpin, J. C., 1992, *Primer on Composite Materials Analysis*, Technomic Publishing Co., Lancaster, PA.
[26] Katz, J. L., and Ukraincik, K., 1971, "On the Anisotropic Elastic Properties of Hydroxyapatite," J. Biomechanics, **4**, pp. 221–227.
[27] Folkes, M. J., and Russell, D. A. M., 1980, "Orientation Effects During the Flow of Short-fibre Reinforced Thermoplastics," Polymer, **21**, pp. 1252–1258.
[28] Toll, S., and Andersson, P.-O., 1991, "Microstructural Characterization of Injection Moulded Composites Using Image Analysis," Composites, **22**, pp. 298–306.
[29] Bay, R. S., and Tucker, III, C. L., 1992, "Fiber Orientation in Simple Injection Moldings. Part II: Experimental Results," Polym. Compos., **13**, pp. 332–341.
[30] Bay, R. S., and Tucker III, C. L., 1992, "Stereological Measurement and Error Estimates for Three-Dimensional Fiber Orientation," Polym. Eng. Sci., **32**, pp. 240–253.
[31] Espinoza Orías, A. A., Deuerling, J. M., Landrigan, M. D., Renaud, J. E., and Roeder, R. K., 2009, "Anatomic Variation in the Elastic Anisotropy of Cortical Bone Tissue in the Human Femur," J. Mech. Behav. Biomed. Mater., **2**, pp. 255–263.
[32] Rudy, D. J., Deuerling, J. M., Espinoza Orías, A. A., and Roeder, R. K., 2011, "Anatomic Variation in the Elastic Inhomogeneity and Anisotropy of Human Femoral Cortical Bone Tissue is Consistent Across Multiple Donors," J. Biomechanics, **44**, pp. 1817–1820.
[33] Cullity, B. D., 1978, *Elements of X-ray Diffraction*, 2nd ed., Addison Wesley Publishing Co., Reading, MA.
[34] Camacho, C. W., Tucker, III, C. L., Yalvaç, S., and McGee, R. L., 1990, "Stiffness and Thermal Expansion Predictions for Hybrid Short Fiber Composites," Polym. Compos., **11**, pp. 229–239.
[35] Hine, P. J., Duckett, R. A., and Ward, I. M., 1993, "Modelling the Elastic Properties of Fibre-Reinforced Composites: II Theoretical Predictions," Compos. Sci. Technol., **49**, pp. 13–21.
[36] Gusev, A., Heggli, M., Lusti, H. R., and Hine, P. J., 2002, "Orientation Averaging for Stiffness and Thermal Expansion of Short Fiber Composites," Adv. Eng. Mater., **4**, pp. 931–933.